PAPER • OPEN ACCESS

Finite magnetic well effects on resistive and drift-resistive ballooning modes in a shaped tokamak

To cite this article: D. Brunetti *et al* 2022 *Nucl. Fusion* **62** 076016

OPEN ACCESS
IOP Publishing | International Atomic Energy Agency Nuclear Fusion
Nucl. Fusion **62** (2022) 076016 (10pp) https://doi.org/10.1088/1741-4326/ac5f7c

Finite magnetic well effects on resistive and drift-resistive ballooning modes in a shaped tokamak

D. Brunetti[1,*], C.J. Ham[1], S. Saarelma[1], J.P. Graves[2], J.W. Connor[1] and A. Kleiner[3]

[1] UKAEA-CCFE, Culham Science Centre, Abingdon, Oxon, OX14 3DB, United Kingdom of Great Britain and Northern Ireland
[2] École Polytechnique Fédérale de Lausanne (EPFL), Swiss Plasma Center (SPC), CH-1015 Lausanne, Switzerland
[3] Princeton Plasma Physics Laboratory, Princeton University, Princeton, NJ 08543, United States of America

E-mail: daniele.brunetti@ukaea.uk

Received 27 January 2022, revised 15 March 2022
Accepted for publication 21 March 2022
Published 29 April 2022

Abstract
The impact of plasma shaping through magnetic well modifications on the stability of resistive ballooning modes (RBMs) in tokamaks is analysed, also including finite diamagnetic flows. Various limiting cases of the dispersion relation, obtained by matching the ballooning equation across the ideal and resistive layers, are analysed. It is found that stability is generally improved by the combination of vertical elongation and positive triangularity, although, in some cases, the growth rate of the unstable mode can be enhanced by these effects. Usually, vertically elongated plasmas with no triangularity are prone to exhibit worse stability properties. A value for the critical β above which RBMs are driven unstable is identified, and a connection with type-III ELM activity is established.

Keywords: MHD, tokamak, resistive ballooning, type-III ELMs

(Some figures may appear in colour only in the online journal)

1. Introduction

H-mode tokamak plasmas are typically characterised by an edge transport barrier [1, 2], in which temperature and density abruptly decrease within a narrow region. As such, large pressure gradients develop which in turn destabilise edge fluctuations called edge localised modes (ELMs). One of the mechanisms that limit the achievable pedestal height is the cycle of pressure drop and subsequent recovery due to ELMs destabilisation. Various types of ELMs are observed depending on pedestal parameters (i.e. temperature and density) [3], the most dangerous ones being the so called type-I ELMs. These events are associated with violent eruptions of energy and particles which deposit significant heat loads on the plasma facing components (PFCs). These heat loads will be intolerable for a steady state reactor and significant research efforts have been directed at developing scenarios without type-I ELMs.

In the eventuality that ELMs cannot be avoided, a scenario with H-mode performance without large ELMs is the type-III ELMy operating regime [3–7]. Type-III ELMs are characterised by a high repetition rate associated with lower heat and particle loads on the PFCs compared to type-I ELMs regimes, and are usually observed above the L $\rightarrow$ H transition boundary [8, 9] at high pedestal collisionality [3, 10–12]. A coherent magnetic precursor oscillation of toroidal mode number

* Author to whom any correspondence should be addressed.

$n \approx 5$–15 is often observed [12–15]. These perturbations tend to occur below the marginal boundary of peeling ballooning modes and disappear as the input power, and therefore temperature, is increased [10, 13]. This suggests that type-III ELMs may be resistive in nature, and indeed several works pointed to the importance of resistive effects on edge modes [16–19].

The most likely magnetohydrodynamic (MHD) instabilities that could explain such behaviour are the resistive ballooning modes (RBMs) [8, 20]. Contrarily to ideal ballooning modes which exhibit two stability regions one at low and the other at high pressure (*first* and *second* stability regions respectively) [21, 22], RBMs are generally found to be unstable all the way across the first ideal stability region [23, 24], whereas they are mainly stable in the second one. This would predict that they should be always observed if the pressure is sufficiently low, which is in contrast with experimental observations [8]. However, an island of stability at low pressure can be accessed if finite magnetic well corrections are included [21, 25–28]. These contributions, which are stronger for moderate n values typically associated with type-III ELM precursors [12–15], may therefore have a significant role. It is important to point out that plasma shaping has a strong impact on the magnetic well [29, 30], improving the pedestal performances, and indeed higher pedestal pressures were sustained at high triangularity in type-I and type-III ELMy regimes [8, 31]. Additionally, diamagnetic flows are known to be an important stabilisation mechanism, and these are likely to be generated in the pedestal where strong gradients develop in H-mode scenarios.

Hence, the aim of this paper is to investigate the role of magnetic well effects, primarily through plasma shaping, on the stability of RBMs, providing a physical understanding of the type-III ELM phenomenon and potentially a scaling for the pedestal height. Indeed, the accessibility of a stability window in the ideal ballooning first stable domain, i.e. at low pressure, could explain why type-III ELMs are observed after the pedestal pressure reaches a threshold value and not before. Note also that the type-III ELMs high repetition rate is likely to be associated with a lower pressure threshold driving the instability [12]. The analytical calculations presented in this work also include finite Larmor radius (FLR) corrections, which may become significant when strong edge gradients (in temperature and density) develop and for sufficiently large n toroidal mode numbers (even for moderate diamagnetic flows). Finally, by employing the EPED model [32, 33] for the pedestal width, we aim to derive an explicit expression, which depends upon macroscopic plasma parameters e.g. pedestal temperature and density, of the RBM marginal boundary. Hence, we identify the type-III ELMs boundary in the density–temperature parameter space, by linking it to RBM, and to some extent ideal ballooning mode, dynamics.

The logic of the mathematical derivation presented in this work is the following: we first focus, within the drift-MHD model, on the description of the equilibrium of a shaped tokamak. Then, we introduce the resistive ballooning equations. These are radially Fourier transformed infernal type equations [22, 34] for which neighbouring high-n harmonics have the same radial shape, although peaking at adjacent rational surfaces. With a careful ordering of pressure gradient, magnetic shear and shaping effects, the ballooning equations can be simplified with the method of averaging. The solution of the resistive ballooning equations yields a dispersion relation which is examined asymptotically near the marginal boundary, and deep inside of the stable/unstable region of the ideal mode. Finally, the associated stability boundaries are expressed in terms of the relevant physical parameters (specifically magnetic shear and pressure gradient).

Thus, the paper is organised as follows: in section 2 the MHD model and plasma equilibrium for a shaped tokamak are discussed. The derivation of the ballooning equation, involving an average over the poloidal variation of the equilibrium, is discussed in section 3, in which a two-region analysis is carried out. The discussion of various limiting cases for the stability boundaries obtained from the dispersion relation, which closely follows the approach of references [35, 36], is the main aim of section 4, and the connection of the analytical results with the experimental observation of type-III ELMs activity is proposed in section 5. Finally, in section 6 a discussion of the results and future outlook is given.

2. MHD model and equilibrium

It is convenient here to provide a brief summary of the physical framework within which the stability analysis will be carried out. Plasma evolution is assumed to obey the resistive drift-MHD equations [37, 38]:

$$\rho\left(\partial_t \boldsymbol{v} + \boldsymbol{v}\cdot\nabla\boldsymbol{v} + \boldsymbol{v}^*\cdot\nabla\boldsymbol{v}_\perp\right) = -\nabla p + \boldsymbol{J}\times\boldsymbol{B}, \tag{1}$$

$$\partial_t \boldsymbol{B} = \nabla\times(\boldsymbol{v}\times\boldsymbol{B}) - \eta\nabla\times\boldsymbol{J} + \frac{m_\mathrm{i}}{e_\mathrm{i}}\nabla\times\left(\frac{\nabla_\parallel p_\mathrm{e}}{\rho}\right), \tag{2}$$

$$\partial_t p + \boldsymbol{v}\cdot\nabla p + \frac{5}{3}p\nabla\cdot\boldsymbol{v} = 0, \tag{3}$$

$$\partial_t \rho + \nabla\cdot(\rho\boldsymbol{v}_\mathrm{i}) = 0, \tag{4}$$

where $\boldsymbol{v}$ and $\boldsymbol{v}^* = m_\mathrm{i}\boldsymbol{B}\times\nabla p_\mathrm{i}/(e_\mathrm{i}\rho B^2)$ (m_i and e_i are the ion mass and electric charge) are the plasma MHD and ion diamagnetic velocities respectively with $\boldsymbol{v}_\mathrm{i} = \boldsymbol{v} + \boldsymbol{v}^*$, ρ is mass density, $\boldsymbol{J} = \nabla\times\boldsymbol{B}$ the current density having been normalised to $\mu_0 = 1$, p_i and p_e the ion and electron pressure respectively with the total pressure denoted by p and η the plasma resistivity which is assumed constant. The symbol $\perp$ indicates the vector projection perpendicular to the magnetic field, i.e. $\boldsymbol{v}_\perp = \boldsymbol{B}\times(\boldsymbol{v}\times\boldsymbol{B})/B^2$ while $\nabla_\parallel = \boldsymbol{b}(\boldsymbol{b}\cdot\nabla)$ with $\boldsymbol{b} = \boldsymbol{B}/B$. Here we assume that the plasma is sufficiently collisional so that at equilibrium $T_\mathrm{e} = T_\mathrm{i}$. Note that the high collisionality assumption allows us to neglect bootstrap corrections to the total toroidal current. We point out that in equation (2) we assumed $\boldsymbol{B}\cdot\nabla T_\mathrm{e} \approx 0$ representing rapid thermal conduction along the magnetic field.

Let us consider a large aspect ratio tokamak ($\varepsilon = a/R_0 \ll 1$ where R_0 and a are the major and minor radii respectively) with a D-shaped cross-section [39]. Let (r, ϑ, φ) be a right handed coordinate system with r a flux label with the dimensions of length, and ϑ (counter-clockwise) and φ the poloidal

and toroidal angles respectively. The equilibrium magnetic field in the plasma is $\boldsymbol{B} = F\nabla\varphi - \nabla\psi \times \nabla\varphi$ where ψ is the poloidal flux. Note that in the limit of a strong longitudinal magnetic field, the equilibrium diamagnetic flow is primarily in the poloidal direction.

In a low-$\beta = 2p/B_0^2 \sim \varepsilon^2$ plasma (B_0 is the equilibrium magnetic field strength on the axis), the equilibrium state ($\partial_t \to 0$) without MHD flows is described by the equation

$$\nabla p = \boldsymbol{J} \times \boldsymbol{B}. \tag{5}$$

For a sufficiently small magnetic shear, the equation above is solved at leading order by [34, 39–41]

$$R = R_0 + r\cos(\theta + r\frac{\delta}{a}\sin\theta) - \Delta, \qquad Z = \kappa r \sin\theta \tag{6}$$

where $\kappa \sim 1$ and $\delta \sim \varepsilon$ describe plasma elongation and triangularity respectively, with the Shafranov shift $\Delta \sim \varepsilon a$ given by ($'\equiv \mathrm{d}/\mathrm{d}r$)

$$\Delta'' + \frac{3}{r}\Delta' + \frac{4}{1+3\kappa^2}\left(\frac{2q^2R_0p'}{rB_0^2} + \frac{2\delta}{a} - \frac{\kappa^2}{R_0}\right) = 0.$$

Here $\psi' = rB_0\kappa/q$ and $F = B_0R_0(1 - \frac{r^2(1+\kappa^2)}{2q^2R_0^2} - \frac{p'}{B_0^2})$.

If we consider the equilibrium poloidal ion velocity to be small, a MHD flow generated by $\boldsymbol{E} \times \boldsymbol{B}$ drifts may be introduced (this would rotate primarily in the poloidal direction counter to the diamagnetic flow). In this case, the equilibrium state is still described with a sufficient accuracy by equation (5) with $p \approx p(r)$. However, the main effect of this additional flow is to introduce a Doppler shift in the eigenfrequency without altering the stability properties. As such, for the sake of simplicity, we will not consider MHD flows at equilibrium.

Introducing the rectified angle ϑ related to the parametrisation (6) via $\theta = \vartheta + \lambda(r,\vartheta)$ with $\lambda = -(r/R_0 + \Delta')\sin\vartheta$, the metric tensor elements $g_{i,j}$ in the straight field line coordinate system (r,ϑ,ϕ) with Jacobian g can be easily derived to the required accuracy by means of (6). The derivation of the stability equations will be the aim of the next section.

3. Ballooning equations

With an axisymmetric equilibrium, the toroidal mode n is a good quantum number, thus for any perturbed quantity $\tilde{f}$ we have

$$\tilde{f} = \sum_m f_m(r)\exp[\mathrm{i}(m\vartheta - n\varphi) + \gamma t].$$

Under the assumption $n \gg 1$ (which also implies $m \gg 1$ with $q \sim \mathcal{O}(1)$ so that $k_\parallel R_0 q \ll 1$ with $k_\parallel$ denoting the parallel wave vector), the perturbation is sufficiently localised so that the quantities q', p' and $s = rq'/q$ can be taken constant. It follows that adjacent resonances (each resonance denoted by r_m for a generic poloidal mode number m) are evenly spaced, i.e. $(r_{m+1} - r_m)/r_m = d = 1/(nqs)$. In addition, we assume that different Fourier harmonics have similar amplitude (i.e. $f_m \sim f_{m+1}$) and impose translational invariance [42]:

$$f_{m+1}(x+d) = f_m(x), \tag{7}$$

with $x = (r - r_m)/r_m$.

Hence, for a given Fourier poloidal harmonic with mode number ℓ, it is convenient to distinguish two regions: one far from its own resonance for which plasma inertia, resistivity and diamagnetism are neglected, and a second one close to r_ℓ where these effects are instead retained. Let us start analysing the region far from resonance.

3.1. Ideal region

After linearising (1), simple algebra yields [41, 43] (hereafter quantities without a tilde are assumed to take their respective equilibrium values)

$$\boldsymbol{B}\cdot\nabla\frac{\tilde{J}^\varphi}{B^\varphi} + \tilde{\boldsymbol{B}}\cdot\nabla\frac{J^\varphi}{B^\varphi} - \boldsymbol{J}\cdot\nabla\frac{\tilde{B}^\varphi}{B^\varphi} - \nabla\varphi\cdot\nabla\frac{1}{B^\varphi}\times\nabla\tilde{p} = I, \tag{8}$$

where the inertia operator I is given by

$$I = \nabla\varphi\cdot\nabla\times\frac{\rho}{B^\varphi}(\gamma\tilde{\boldsymbol{v}} + \boldsymbol{v}^*\cdot\nabla\tilde{\boldsymbol{v}}_\perp).$$

In this region we let $I \to 0$.

Let us introduce the ballooning parameter $\alpha = -2R_0p'q^2/B_0^2$ and assume that the perturbation is localised near the plasma edge. In this region one usually has $s \sim \alpha \sim 1$, which is the standard ordering employed in the usual $s-\alpha$ model [44]. Within this model, field line bending and coupling with the nearest neighbouring sidebands arising from the first and the last two terms in (8) are of the same order. However, dealing with shaping effects, which requires higher order expansions of the metric coefficients and a more careful analysis of the poloidal couplings (i.e. for a given mode m we must retain up to the $m \pm 4$ sidebands), is significantly more difficult.

Thus, in order to simplify the algebra involved, we take $s, \alpha \ll 1$ [21, 45] and expand each term of (8) to the relevant order by including pressure and elongation driven couplings. Note that this is consistent with the equilibrium calculation presented in the previous section. The equations derived with this approximation do not differ too much from the ones obtained using the $s \sim \alpha \sim 1$ ordering. It is worth noting that the stability boundaries, at least for the ideal case, calculated in the limit $s \ll 1$ behave qualitatively in a similar manner to the ones obtained by more precise numerical computations with realistic profiles [22, 46]. This suggests that our model could be employed, to some extent, for cases with $s \sim \alpha \sim 1$ [47].

We immediately notice that because of the translational invariance (7), it is sufficient to compute only a single Fourier projection of equation (8), say the mth with the resonance denoted by r_m. Thus, equations (2) and (3) give $\sqrt{g}\tilde{B}^r_m = \mathrm{i}r\kappa B_0(m/q - n)X_m$ with $\tilde{p}_m = -p'X_m$ where $X_m = \tilde{v}^r_m/\gamma$. Plasma compressibility has been neglected. Let us define

$$Y_m = (\sqrt{g}\tilde{B}^r)_m/(\mathrm{i}r\kappa B_0).$$

We take $r\,\mathrm{d}\ln\tilde{f}/\mathrm{d}r \sim m$ so that $(m/q - n) \approx -snx$ where $nx \sim 1$ and x has been defined in equation (7). From the covariant toroidal projection of (1) it is easy to show

that $(\tilde{B}_\varphi)_m \approx \frac{R_0 p'}{B_0} X_m$, so that using $\nabla \cdot \tilde{\boldsymbol{B}} = 0$ one has $(\sqrt{g}\tilde{B}^\vartheta)_m = -\mathrm{i}/m(\sqrt{g}\tilde{B}^r)'_m$.

The equation for the perturbation in the ideal region is obtained by multiplying (8) by $\sqrt{g}$ and selecting the mth Fourier component. Couplings between the nearest $m \pm 1$ harmonics are generated by the last term on the left-hand side in (8), whereas the third one, which also combines with the fourth, is associated with the magnetic well [29, 30]. Additional elongation driven couplings with the $m \pm 2$ harmonics arise from the first term which also yields the familiar terms in the Newcomb equation [48]. Finally, the term proportional to the equilibrium current density gradient can be neglected. Thus, under the assumption that the mode is localised near the plasma edge for which $r \approx r_m \approx a$, we eventually obtain

$$\frac{\mathrm{d}}{\mathrm{d}x}\left(x^2\frac{\mathrm{d}X_m}{\mathrm{d}x}\right) - (m^2x^2 + \frac{\bar{\alpha}}{s^2}U)X_m + \frac{\bar{\alpha}}{2ms^2}\sum_{\ell=m\pm1}\left(mX_\ell \pm \frac{\mathrm{d}X_\ell}{\mathrm{d}x}\right) - \frac{x}{2ns}\left(\frac{\kappa^2-1}{\kappa^2+1}\right) \times \sum_{\ell=m\pm2}\left(\frac{\mathrm{d}^2Y_\ell}{\mathrm{d}x^2} \pm 2m\frac{\mathrm{d}Y_\ell}{\mathrm{d}x} + m^2Y_\ell\right) = 0, \tag{9}$$

where here $Y_\ell = (\ell/q - n)X_\ell$, $\bar{\alpha} = 2\alpha/(1+\kappa^2)$ and

$$U = \frac{a}{2R_0}\left(\frac{1+7\kappa^2}{1+3\kappa^2} - \frac{1+\kappa^2}{q^2}\right) + \bar{\alpha}\frac{1+\kappa^2}{1+3\kappa^2} + \frac{3\delta(\kappa^2-1)}{1+3\kappa^2}.$$

In the limit $s^2 \sim \alpha$ [21, 45], required to have comparable field line bending and coupling contributions, the term U in equation (9) is formally smaller compared to other contributions, which are all of the same order. However, in experiments both aspect ratio and shaping parameters, i.e. $\kappa - 1$ and δ, may take values not much smaller than unity, suggesting that such corrections may enter the problem in leading order, that is the term with U may be of the same order as the field line bending and coupling ones. Consequently, we retain the U term. It is also worth pointing out that the ratio of poloidal to radial derivatives in (9) is expected to scale as $md \sim 1/s$, and, although the magnetic shear is supposed to be small (cf section 2), both contributions are taken into account. Hence, we envisage that our model could be potentially extended to $s \sim 1$ cases. A method for solving (9) with $s \sim 1$ is given in reference [49].

We now Fourier decompose the displacement X_m by defining $X^\dagger_m(k) = \int_{-\infty}^{\infty}\mathrm{d}x\, X_m(x)\exp(-\mathrm{i}kx)$, and take the kth moment of equation (9). Hereafter the dagger symbol will denote a k-space Fourier transformed quantity. By exploiting the radial symmetry of the perturbation given by (7) with $m \approx nq$, after some straightforward algebra we finally obtain

$$\frac{\mathrm{d}}{\mathrm{d}y}\left\{[1+y^2 + \left(\frac{\kappa^2-1}{\kappa^2+1}\right)(1+y^2-2h^2(y))]\frac{\mathrm{d}X^\dagger_m}{\mathrm{d}y}\right\} + \frac{\bar{\alpha}}{s^2}[h(y) - U]X^\dagger_m = 0, \tag{10}$$

having defined $h(y) = y\sin\frac{y}{s} + \cos\frac{y}{s}$ and $y = k/m$. Equation (10) features two length scales, the short one being contained in the oscillating coefficients of the function h. The solution of the equation above can be obtained by means of the *averaging method* [50–53] (a very readable account of this method is given in references [37, 54]).

Let us define $e = (\kappa^2-1)/(\kappa^2+1)$ and $\chi = y/s$. Introducing the smallness parameter λ, we set [21, 54]

$$e \sim \alpha \sim \lambda, \qquad s \sim \delta \sim \lambda^2, \qquad \varepsilon \sim \lambda^3,$$

and expand the function $X^\dagger_m$ as follows:

$$X^\dagger_m = \xi_0(y) + \lambda\xi_1(y,\chi) + \lambda^2\xi_2(y,\chi) + \cdots, \tag{11}$$

with the requirement that the functions $\xi_1, \xi_2, \ldots$ vanish when averaged in the variable χ over a period of 2π. Thus, writing $\mathrm{d}/\mathrm{d}y \to \partial_y + \frac{1}{s}\partial_\chi$, equation (10) is solved order by order in λ, from λ^{-3} to λ^{-1}, providing an expression for ξ_i $(i = 1, 2, 3)$. These are then plugged into the zeroth order (in λ) of (9), and averaging over χ yields an equation for ξ_0. With the help of computer assisted algebra tools [55], the final result reads [21, 29]

$$\frac{\mathrm{d}}{\mathrm{d}y}\left[(1+y^2)\frac{\mathrm{d}\xi_0}{\mathrm{d}y}\right] - \left[\nu(\nu+1) - \frac{b^2}{1+y^2}\right]\xi_0 = 0, \tag{12}$$

with $\nu(\nu+1) = \frac{\alpha}{s^2}[\varepsilon(1-1/q^2) + \frac{3}{2}e\delta - \frac{\alpha}{8}e^2]$ and $b^2 = \frac{\alpha^2}{s} - \frac{7}{32}\frac{\alpha^4}{s^2}$. We shall restrict our attention to the case $0 < \nu < 1/2$, i.e. for resistive interchange stable configurations. If we allowed $s \sim \alpha \sim 1$ [44] in the derivation of the mode equation (9), the averaging procedure would have an equation similar to (12) with the last term on the left-hand side replaced by $(2\alpha^2/s - \frac{3}{8}\alpha^4/s^2)/(1+y^2)^2$ [47, 54]. This fully provides a description of the perturbation dynamics in the ideal region. In the next subsection the derivation of the layer equation is presented.

3.2. Inertial-resistive layer

Let us perform our analysis in the proximity of r_m and take $\mathrm{d}/\mathrm{d}x \gg m$. Assuming that $\nabla \cdot \boldsymbol{v}_\mathrm{i} \approx 0$ [56], we may write $\tilde{\rho}_m = -\rho' X_m$ and $\tilde{p}_{\mathrm{i}m} = -p'_\mathrm{i}X_m$ where the ion pressure equation is given by (3) with the replacements $p \to p_\mathrm{i}$ and $\boldsymbol{v} \to \boldsymbol{v}_\mathrm{i}$. Moreover, it easily follows that $(\tilde{v}_\varphi)_{m\pm1} = \frac{1}{\mathrm{i}m}R_0 q(\gamma + \mathrm{i}m\omega_\mathrm{i})\frac{\mathrm{d}X_m}{\mathrm{d}x}$ with $\omega_\mathrm{i} = m_\mathrm{i}p'_\mathrm{i}/(e_\mathrm{i}\rho a\kappa B_0)$. In the inertial layer, plasma compressibility must be retained so that $\tilde{p}_{m\pm1} = -p'X_{m\pm1} + \delta p_{m\pm1}$ where $\delta p_{m\pm1}$ are obtained from the parallel projection of (1), reading at leading order:

$$\delta p_{m\pm1} = \pm\frac{R_0\rho q^2}{m}\frac{\mathrm{d}}{\mathrm{d}x}[\gamma(\gamma + \mathrm{i}m\omega_\mathrm{i})X_m] + p'(X_{m\pm1} \mp qY_{m\pm1}).$$

Neglecting resistivity fluctuations in (2) under the assumption that the perturbation varies sufficiently rapidly in the radial direction, we obtain to the required accuracy

$$[1 + Hy^2(1 + e\cos\frac{2y}{s})]Y^\dagger_m = \frac{s}{\mathrm{i}q}\frac{\mathrm{d}X^\dagger_m}{\mathrm{d}y}, \tag{13}$$

where $H = m^2\eta(1+\kappa^2)/[2\kappa^2 a^2(\gamma - \mathrm{i}m\omega_\mathrm{e})]$ and $\omega_\mathrm{e} = \rho' T_\mathrm{e}/(e_\mathrm{i}\rho a\kappa B_0)$ having included elongation driven couplings.

The coupling between (8) and (13) completely describes the mode dynamics in the resistive layer. We recall that equation (8) must be multiplied by $\sqrt{g}$ before taking the mth poloidal Fourier harmonic. Let us focus on each individual contribution arising from (8). It is easy to see that the term proportional to the gradient of the equilibrium current density is negligible also in this region. The term proportional to the perturbed current density can be easily worked out in line with the derivation of the section before, where here the magnetic fluctuation is given by (13). The pressure driving terms, i.e. the third and fourth on the left-hand side of (8), yield the last term in (10) augmented by the plasma compressibility contribution, which is proportional at leading order to $\frac{\mathrm{d}}{\mathrm{d}x}(\delta p_{m-1} - \delta p_{m+1})$. Finally, the inertial contribution can be written as $(\sqrt{g}I)_m \propto \gamma(\gamma + \mathrm{i}m\omega_\mathrm{i})\frac{\mathrm{d}^2}{\mathrm{d}x^2}[X_m + \frac{e}{2}\sum_{\ell=m\pm2} X_\ell]$. Therefore, collecting these results together and transforming to the k-space yields

$$\frac{\mathrm{d}}{\mathrm{d}y}\left[f(y)\frac{\mathrm{d}X_m^\dagger}{\mathrm{d}y}\right] + \left(\frac{\bar\alpha}{s^2}[h(y)-U] - [\zeta(y) + \frac{(2qy)^2}{1+\kappa^2}]\Lambda^2\right)X_m^\dagger - \frac{\bar\alpha}{s}\left(\frac{H\zeta(y)}{1+H\zeta(y)}\right) y\cos\frac{y}{s}\frac{\mathrm{d}X_m^\dagger}{\mathrm{d}y} = 0, \tag{14}$$

where we defined $\zeta(y) = y^2[1 + e\cos\frac{2y}{s}]$ and $\Lambda^2 = \gamma(\gamma + \mathrm{i}m\omega_\mathrm{i})q^2/(s^2\omega_\mathrm{A}^2)$, $\omega_\mathrm{A} = B_0/(R_0\sqrt{\rho})$, with the function $f(y)$ given by

$$f(y) = \frac{1 + y^2 + e[1 + y^2 - 2h(y)^2]}{1 + H\zeta(y)}.$$

Note that for the two-regions analysis to be valid, we require that $n^2 \ll a^2|\gamma - \mathrm{i}m\omega_\mathrm{e}|/(s^2q^2\eta)$, where this condition must hold also when $s \sim 1$, introducing an effective upper limit in n [27]. Thus, we must restrict our analysis to moderate n modes only.

We perform a two-scales analysis [57] similarly to the derivation in the ideal region. Let us employ the variable χ for the argument of the periodic coefficients in the equation above (cf section before), and take λ as a smallness parameter. We order $H \sim \lambda^2$, $\gamma \sim m\omega_\mathrm{i,e} \sim \lambda$ with $y \sim 1/\lambda$ and substitute $\mathrm{d}/\mathrm{d}y \to \lambda\partial_y + \frac{1}{s}\partial_\chi$. Here, no λ-ordering is introduced for magnetic shear and shaping parameters. The eigenfunction $X_m^\dagger$ is expanded in λ according to (11), and then plugged into (14) yielding an expression of the form

$$\lambda^{-1}\mathfrak{D}_{-1}(\xi_0,\xi_1) + \mathfrak{D}_0(\xi_0,\xi_1,\xi_2) + \cdots = 0.$$

It is trivial to verify that the dependence upon ξ_2 in $\mathfrak{D}_0$ is annihilated by averaging in χ over a period of 2π. The leading order of the equation above provides an expression for ξ_1. Elongation introduces complicated angular dependencies in the variable χ which are resolved by casting ξ_1 as $\xi_1 = \Xi^{(0)} + e\Xi^{(1)} + \cdots$ (obviously $\Xi^{(i)}$ must be periodic in χ) and then performing a perturbative expansion in e of the expressions $\mathfrak{D}_{-1} = 0$ and $\int_0^{2\pi}\mathfrak{D}_0\,\mathrm{d}\chi = 0$. For the accuracy required in our calculations, it is sufficient to compute $\Xi^{(j)}$ with $j = 0, 1, 2$ (this is for a correct estimate of the magnetic well). After a considerable amount of algebra, taking δ and therefore magnetic well contributions sufficiently small and expanding to second order in e gives

$$\frac{\mathrm{d}}{\mathrm{d}y}\left(\frac{y^2}{1+H_0y^2}\frac{\mathrm{d}\xi_0}{\mathrm{d}y}\right) - [\nu(\nu+1) + y^2\Lambda_\mathrm{i}^2]\xi_0 = 0, \tag{15}$$

with $H_0 = 2\kappa H/(1+\kappa^2)$ and

$$\Lambda_\mathrm{i}^2 = \left(\frac{1 + 2(1-e)q^2}{1 - e^2/2}\right)\Lambda^2 \equiv \frac{\kappa^2}{\sigma}(1+2q^2)\Lambda^2,$$

where in this expression, which defines the quantity σ, we may let q be large.

Equation (15) incorporates shaping and FLR effects in the inertial layer, and together with (12) determines the ballooning dynamics. Their solution and the associated dispersion relation are discussed in the next section.

4. Stability boundaries

Throughout this section we let $m = nq$ and rescale $\omega_\mathrm{A} \to \omega_\mathrm{A}/\sqrt{1+2q^2}$. The solutions of equations (12) and (15) are well known [25, 26, 41, 53] and from their matching over the overlapping region in y we obtain the dispersion relation. Although (12) yields even and odd solutions, we restrict our attention to even parity modes only. Thus, the dispersion relation reads [25, 38, 41]

$$\frac{1}{\lambda_\mathrm{H}} \equiv \frac{\Gamma[\frac{1}{2}(1-b+\nu)]\Gamma[\frac{1}{2}(1+b+\nu)]\Gamma^2[-\nu-\frac{1}{2}]}{\Gamma[-\frac{1}{2}(b+\nu)]\Gamma[\frac{1}{2}(b-\nu)]\Gamma^2[\nu+\frac{1}{2}]} = (H_0Q)^{-\nu-\frac{1}{2}}\frac{Q+\nu}{Q-\nu-1}\frac{\Gamma\left[\frac{1}{4}(Q+3-2\nu+\nu(\nu+1)/Q)\right]}{\Gamma\left[\frac{1}{4}(Q+5+2\nu+\nu(\nu+1)/Q)\right]} \tag{16}$$

where $Q = \Lambda_\mathrm{i}/\sqrt{H_0}$ and Γ is the Gamma function [58]. Although this equation is rather complicated, some limiting cases can be identified and addressed analytically.

Since $Q \sim \eta^{-1/2}$, the ideal limit is trivially obtained by taking $Q \to \infty$, providing an expression for the mode marginal stability boundary, which, for small diamagnetic ion flow, reads [41]

$$b \approx 1 + \nu + (1 - \frac{e}{2})q|m\omega_\mathrm{i}|/(s\pi\omega_\mathrm{A}).$$

The destabilising role of the elongation is evident through the weakening of the diamagnetic contribution, although its interaction with triangularity improves stability via magnetic well corrections contained in the ν term [51].

Focussing on the resistive case, equation (16) can be analysed asymptotically for some limiting values of λ_H. This quantity, defined by the left-hand side of (16), is a function of the equilibrium parameters and its value determines Q, i.e. the growth rate. Roughly speaking, λ_H can be considered as a measure of the proximity to the $s-\alpha$ stability boundary [38, 59]. The three cases of interest are: (i) $\lambda_\mathrm{H} > 0$, (ii) $\lambda_\mathrm{H} \sim 0$, and (iii) $|\lambda_\mathrm{H}| \ll 1$ with λ_H negative. These correspond respectively to analysing the deeply unstable, marginally stable and

deeply stable regions of the ideal mode without diamagnetic effects. Thus, balancing λ_H with the right-hand side of (16) yields the three limits $Q \gg 1$, $Q \sim 1$, and $Q \ll 1$. These cases are analysed below.

4.1. $Q \gg 1$ regime

Let us take $\lambda_H > 0$ with $\omega_i \neq 0$ and assume that the analysis is carried out in a neighbourhood of the stability region of the ideal mode when ion diamagnetic flows are present. Expanding equation (16) for large Q yields to leading order

$$\Lambda_i^2 - 4\lambda_H^{2/(1+2\nu)} \approx \left(\frac{5}{2} - \frac{\nu}{3}\right) H_0, \tag{17}$$

where on the right-hand side we assumed $\nu \ll 1$ which holds for weak shaping with a sufficiently large aspect ratio. The marginal stability boundary of the ideal mode is recovered by setting $H_0 \to 0$. We shall stress that equation (17), and similarly other simplified expressions of the full dispersion relation, only picks out a limited number of all the roots generated by (16).

Let us introduce the Lundquist number $S \gg 1$ defined as $S = a^2\omega_A/\eta$ and assume q large enough. Therefore, near the stability boundary of the ideal mode with diamagnetic flows, if we substitute $\gamma \to \gamma - im\omega_i/2$ with $\gamma \ll |m\omega_i|$ in equation (17) we find

$$\gamma \approx \gamma_* \left[1 - \frac{\nu}{15} + \frac{\gamma_I^2}{\gamma_*^2}\right],$$

where

$$\gamma_* \approx \frac{\sqrt{5}}{2}[m|\omega_e + \omega_i/2|/\omega_A^3]^{-1/2}[s^2m^2/(q^2S)]^{1/2},$$
$$\gamma_I^2 \approx (1+e)[\lambda_H^{1/(1+2\nu)} s\omega_A/q]^2 - (m\omega_i/4)^2 < 0,$$

with $-\gamma_I^2 \ll \gamma_*^2$. The growth rate, which is rather fast since it scales as $1/\sqrt{S}$, decreases as λ_H is reduced. Further stabilisation, although small, is gained by ν effects. With ω_i sufficiently small, the marginal boundary is given by the following expression

$$b = 1 + \nu + \frac{q|m\omega_i|}{s\pi\omega_A}\left(1 - \frac{e}{2} - \frac{10s^2\omega_A^3(mS)^{-1}}{\omega_i^2|\omega_e + \omega_i/2|}\right). \tag{18}$$

The destabilising role of the resistivity is clearly evident, although modes with a sufficiently large n are expected to be completely suppressed by the ion diamagnetic flow. We point out that if S is large enough, the stability boundary identified by (18) is not too far away from the one of the ideal mode. This seems to indicate that a modest heating may suppress these instabilities.

Finally, it is worth noticing that if γ_I^2 is sufficiently large and negative with $\lambda_H > 0$ not small, the two roots with frequency $-i\omega_i/2 \pm \sqrt{\gamma_I^2}$ are both stable.

4.2. $Q \sim 1$ regime

This case holds when $|\lambda_H| \ll 1$, i.e. close to the ballooning ideal marginal boundary without diamagnetic effects. We first expand the right-hand side of (16) to first order in $\nu \ll 1$ and then take the limit $Q - 1 \ll 1$. This yields

$$\frac{1}{\lambda_H} = \frac{2}{(Q-1)\sqrt{\pi H_0}}\left(1 + \frac{\nu}{Q-1}\right).$$

Note that in the resistive region $H_0 y^2 \sim \Lambda_i^2 y^2 \sim 1$ [21], so that for $y \gg 1$ we obtain $qm^2/(sS) \ll 1$. A straightforward rearrangement of the equation above gives [35, 38, 59] $(\nu/(Q-1) \ll 1)$

$$Q = 1 + \nu + 2\lambda_H/\sqrt{\pi H_0}.$$

Thus, in the limit of vanishing diamagnetic corrections, we find that the growth rate is

$$\gamma = \gamma_R\left[1 + \frac{2}{3}\nu + \frac{4\lambda_H}{3\sqrt{\pi}}\left(\frac{\sigma}{\kappa}\right)^{1/6}\left(\frac{sS}{qm^2}\right)^{1/3}\right], \tag{19}$$

where $\gamma_R \approx \omega_A[s^2m^2/(q^2S)]^{1/3}$. For $S \to \infty$ the stability boundary identified by (19) is $\lambda_H = 0$, in agreement with the findings of the previous section. Stability is improved as λ_H becomes more negative [35], whereas the growth rate is increased by finite magnetic well corrections when $\lambda_H = 0$. It is worth noticing that the stabilising term proportional to λ_H weakens as m increases, although the condition $qm^2/(sS) \ll 1$ must be fulfilled, thence restricting the validity of this result to the neighbourhood of the marginal stability boundary of the ideal mode. Note that the analysis above has been derived in the limit $\nu \ll Q - 1 \ll 1$, yielding $\nu \ll \lambda$ with λ a smallness parameter which determines how close the system is to the marginal boundary of the ideal mode (not to be confused with λ_H). This condition can be fulfilled if the aspect ratio is sufficiently large.

If diamagnetic flows are allowed, the growth rate of the low frequency mode is [35]

$$\gamma = \gamma_{R_*}\left[1 + 2\nu + 4\lambda_H\sqrt{\frac{\kappa S|\omega_e|}{\pi m\omega_A}}e^{i\pi/4}\right], \tag{20}$$

where $\gamma_{R_*} \approx s^2\omega_A^3/(q^2S\omega_i\omega_e)$. Similar conclusions to the ones discussed above can be drawn regarding the stability of this mode. An approximate expression for the stability boundary can be written in a form similar to (18) with the obvious replacements. Note that this root has a rather small growth rate ($\gamma_{R*} \sim S^{-1}$) and it vanishes when $S \to \infty$. As in (19), the stabilising contributions weaken as m increases.

4.3. $Q \ll 1$ regime

Here we take $|\lambda_H| \gg 1$ with $\lambda_H < 0$, i.e. far from the ideal-MHD instability threshold in the ideal ballooning stable region of the $s - \alpha$ space. Let us first neglect diamagnetic corrections. Similarly to the regime discussed in the previous paragraph, we first expand the right-hand side of equation (16) to first order in $\nu \ll 1$ and then take the limit $Q \ll 1$. This yields [28]

$$\frac{1}{|\lambda_H|} = \frac{\Gamma[\frac{3}{4}]}{\Gamma[\frac{5}{4}]} \times \sqrt{\frac{Q}{H_0}}\left(1 + \frac{\pi\nu}{4Q}\right). \tag{21}$$

For vanishing FLR effects $Q \sim \gamma^{3/2}$, $H_0 \sim \gamma^{-1}$, and the equation above corresponds to the one analysed in references [21, 25, 26] augmented by shaping effects. If $\nu \to 0$, the stability boundary for the resistive modes is given by $b = 0$, in accordance with previous analyses [21, 23, 24]. The presence of the interchange term ν, however, introduces a threshold in $1/|\lambda_{\rm H}|$ as pointed out in references [21, 25, 26]. An estimate of such a threshold can be found by assuming ν/Q sufficiently small, so that from (21) one obtains [21]

$$\gamma = \gamma_{\rm T}\left[1 - \nu\left(\frac{|\lambda_{\rm H}|}{C_0}\right)^{6/5}\left(\frac{sS\sqrt{\sigma}}{m^2 q}\right)^{2/5}\right],$$

where $C_0 = (5/\pi)^{5/6}\Gamma[5/4]/\Gamma[3/4] \approx 1.09$ and

$$\gamma_{\rm T} = \omega_{\rm A}\left(\frac{\Gamma[5/4]}{|\lambda_{\rm H}|\Gamma[3/4]}\right)^{4/5} \times \left(\frac{s^2 m^6 \sigma}{q^2 S^3 \kappa^5}\right)^{1/5}.$$

Thus, the result above yields the following expression for the stability boundary

$$|\lambda_{\rm H}| = C_0 \nu^{-5/6}\sigma^{-1/6}\left(\frac{m^2 q}{sS}\right)^{1/3} \equiv \mathscr{A}.$$

Since $\nu \ll 1$, the right-hand side of this equation could take values of order unity. Similarly to the analysis in the previous subsection, the condition $\nu \ll Q \ll 1$ yields $\nu \ll 1/qs^{2/5}$. Because of the complicated Gamma function dependencies in $\lambda_{\rm H}$, it is desirable to identify limits which are sufficiently simple to be dealt with analytically. Hence, if the right-hand side of the equation above is small, we are allowed to expand $|\lambda_{\rm H}|$ to first order in ν giving

$$b = 1 + \nu - \frac{4C_0}{\pi}\nu^{-5/6}\sigma^{-1/6}\left(\frac{m^2 q}{sS}\right)^{1/3}. \qquad (22)$$

It is evident that this boundary lies between the ideal marginal ($b = 1 + \nu$) and the resistive one with $\nu = 0$ ($b = 0$). Conversely, when $\mathscr{A} \sim 1$, we let $\nu \to 0$ in $|\lambda_{\rm H}|$ and obtain

$$\frac{\cot(b\pi/2)}{2b} \approx \frac{1}{\pi b^2} - \frac{\pi}{12} = C_0 \nu^{-5/6}\sigma^{-1/6}\left(\frac{m^2 q}{sS}\right)^{1/3}, \qquad (23)$$

where the approximation above accurately holds when b is sufficiently far from unity. The ideal and the resistive $\nu = 0$ stability boundaries along with the ones identified by equations (22) and (23) are shown in figure 1. At finite ν, a region of stability opens at low α. The transition from (22) to (23) occurs when $\mathscr{A} \sim N$ with $0 \ll N \ll 1$. For a circular torus $\nu \sim \alpha\varepsilon/s^2$, thus letting $C_0 \sim \sigma^{1/6} \sim 1$ yields

$$s \sim N^{3/4}\left(\frac{S}{m^2 q}\right)^{1/4}(\alpha\varepsilon)^{5/8}.$$

Stability is improved at high S, eventually coinciding with the one of the ideal mode, with strong shaping and Mercier contributions, i.e. large ν. This suggests that vertically elongated compact devices with high positive triangularity should exhibit better stability properties against RBMs. It is interesting to note that plasma shaping greatly affects the opening of the RBM stability window at low pressure, whereas for ideal modes such an effect impacts more at low magnetic shear (i.e. at higher edge current densities) [60].

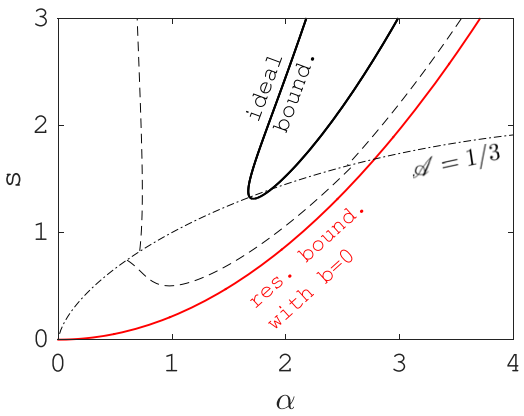

Figure 1. Ideal and resistive stability boundaries for a shaped tokamak with $\varepsilon = 0.05$, $q = 4$, $\kappa = 1.3$, $\delta = 0.1$ and $S = 10^8$. Ideal $n = \infty$ ballooning modes are unstable inside the region delimited by the thick full black line. The red curve identified by the condition $b = 0$ indicates the stability boundary of the $n = 10$ resistive mode with $\nu = 0$ (instability occurs above this curve). At finite ν, the marginal boundary is highlighted by the dashed line: below the $\mathscr{A} = 1/3$ level (highlighted by the dot–dashed line) the resistive boundary at finite ν is computed by means of (22), whereas equation (23) is employed above this level, both indicated by the dashed line. Similarly to the ideal case, instability occurs within the region delimited by the dashed line.

When strong diamagnetic effects are introduced, following the procedure outlined in references [35, 36], from the dispersion relation (16) we obtain

$$\frac{\Gamma[5/4]}{\Gamma[3/4]} \approx \lambda_{\rm H}^{(0)}\frac{\sqrt{Q/H_0}}{Q-1}(1 + \nu \mathfrak{f}(Q)),$$

where $\lambda_{\rm H}^{(0)} = \lambda_{\rm H}(\nu = 0)$. Note that, compared to (21) the equation above retains the $Q - 1$ singularity. The function $\mathfrak{f}(Q)$ can be approximated by assuming Q small, yielding $\mathfrak{f}(Q) \approx \pi/(4Q)$. Thus, under the assumption $Q \sim \nu/Q \ll 1$ we may write

$$\frac{\Gamma[5/4]}{\Gamma[3/4]} \times \frac{1}{|\lambda_{\rm H}^{(0)}|}\left(1 - Q - \frac{\pi\nu}{4Q}\right) = \sqrt{\frac{Q}{H_0}}. \qquad (24)$$

One can immediately verify that for $|\lambda_{\rm H}| \gg 1$ there are three roots. Seeking the unstable root with frequency $m\omega_{\rm e}$, we substitute $\gamma \to \gamma + {\rm i}m\omega_{\rm e}$ with $\gamma \ll |m\omega_{\rm e}|$. Equation (24) can be easily solved perturbatively [36], yielding for the fastest growing mode

$$\gamma \propto 1 - \frac{8}{3}\Omega_* + \frac{\pi\nu}{3\Omega_*}, \qquad (25)$$

where we defined

$$\Omega_* = \left(\frac{\Gamma[5/4]}{\Gamma[3/4]|\lambda_H^{(0)}|}\right)^{2/3} \times \left[\frac{m^2 q^2 \kappa^2 \omega_{\rm e}(\omega_{\rm e} + \omega_{\rm i})}{s^2 \omega_{\rm A}^2 \sigma}\right]^{1/3}.$$

The result above suggests the destabilising effect of finite magnetic well corrections [61, 62]. However, complete stabilisation can be achieved for any m [35, 36] owing to the second term on the right-hand side of (25) for $\lambda_{\rm H}$ sufficiently small. We also point out, that the growth rate scales as S^{-1} [35, 36] indicating that this root grows slowly and eventually disappears in the ideal limit.

Thus, having discussed the physically relevant limits of the dispersion relation (16), the aim of the next section is to link the analytical findings to experimental observations.

5. Critical pressure height

As mentioned in the introduction, RBMs are likely to be associated with type-III ELM dynamics. Hence, our aim in this section is to derive an expression for the critical pedestal pressure height beyond which RBMs appear, and link it to type-III ELM phenomenology. Type-III ELMs are usually found above the L $\rightarrow$ H boundary [8, 9] at moderate pedestal height and high collisionality [3, 10, 12, 13]. Since type-III ELMs are localised in a region of low values of edge current in the peeling-ballooning stability diagram at not too high pressure, we focus on equation (23), i.e. for a low-α and moderate s case. Noting also that the boundaries computed with $s \sim 1$ behave qualitatively as the ones obtained in the $s \ll 1$ limit [22], it might be reasonable, to some extent, to push the theory towards the $s \sim 1$ limit. Finally, because the toroidal wave number associated with type-III ELM precursors is generally not too large ($n \sim 10$) [12–15], we may drop diamagnetic corrections.

The pressure gradient appearing in the ballooning parameter α can be well approximated by

$$-\frac{{\rm d}p}{{\rm d}r} \approx \frac{p}{a\Delta_{\rm ped}},$$

where $\Delta_{\rm ped} = (a - r_{\rm ped})/a$ is the pedestal width with $r_{\rm ped}$ indicating the pedestal shoulder. The quantity $\Delta_{\rm ped}$ is estimated by means of the EPED model [32, 33, 46], in which the pedestal width scales with the pressure according to $\Delta_{\rm ped} = Cq\beta^{1/2}/\varepsilon$ with $C \sim 0.05$ where β has to be evaluated at the pedestal top. For $T_{\rm e} = T_{\rm i} = T$ we have $\beta = 2\mu_0 p/B^2 = 4\mu_0 n_{\rm e} T/B^2$ where $n_{\rm e}$ is the plasma density, having restored the vacuum permeability. Note that we accounted for the fact the EPED-pedestal width is written as a function of the poloidal flux [32, 33], whereas our expression depends upon the variable $r \sim \sqrt{\psi}$. Finally, we take the local value of the Lundquist number as an independent parameter, i.e. the value of resistivity in S is independent of the pedestal top temperature. This is consistent with the derivation in section 3, in which we considered the instability to be highly localised, i.e. $m \gg 1$.

As noted in the previous section, ν corrections to the ideal marginal boundary are rather weak in the region of sufficiently high magnetic shear. This, indeed, might explain why the transition temperature between type-I and type-III ELMy behaviour depends weakly upon triangularity [8]. Therefore, by writing $\alpha = q\sqrt{\beta}/C$, the boundary of the first stability region for the ideal mode with $\nu = 0$ is identified by $b =$ 1 which yields $\beta \approx 1.48 \times sC^2/q^2$. Focussing on the resistive perturbation, if the ratio α^2/s is sufficiently low (low-α/high-s region), we are allowed to take $b^2 \approx \alpha^2/s$. Thus, approximating $\nu^{-5/6} \approx \alpha^{-1}(\nu/\alpha)^{-5/6}$ on the right-hand side of (23), we can obtain an explicit expression for the critical pedestal pressure which reads

$$q\sqrt{\beta}/C \approx -\tau + \sqrt{12s/\pi^2 + \tau^2}, \tag{26}$$

where

$$\tau = \frac{6}{\pi} q s^{4/3} C_0 (\varepsilon + \frac{3}{2} e\delta)^{-5/6} \sigma^{-1/6} \left(S/n^2\right)^{-1/3},$$

having neglected the $e^2\alpha/8$ term in ν (this is because α is assumed to be small enough) with $q \gg 1$. An example of the behaviour of the stability boundary identified by (26) in the $n_{\rm e} - T$ parameter space, which exhibits qualitative similarities with experimental findings [8, 9, 31], is shown in figure 2. The beneficial role of plasma shaping, i.e. vertical elongation with positive triangularity, is apparent through the upwards shift of the RBM stability boundary. We point out that type-I ELMs are likely to appear as the boundary of the ideal mode is met, thus limiting the maximum achievable pressure height [20]. As such, we argue that the boundary of the second stability region is never crossed. We stress however that diamagnetic flows may favour the accessibility to higher pressure regions. On the other hand, the RBM (and thus the type-III ELMs) threshold is a *softer* limit which can be crossed allowing higher pressure regions to be explored, until the type-I ELM boundary is reached.

We shall now briefly discuss the boundaries identified by equations (18) and (22), both of which share the same structure. By taking S large, we note that although (20) yields a similar expression for the stability boundary, the growth rate associated with this mode is so small ($\sim S^{-1}$) as to be not particularly relevant in the limit of large Lundquist numbers. Hence, taking $\frac{7}{32}\alpha^2/s \ll 1$ and neglecting the $e^2\alpha/8$ term in

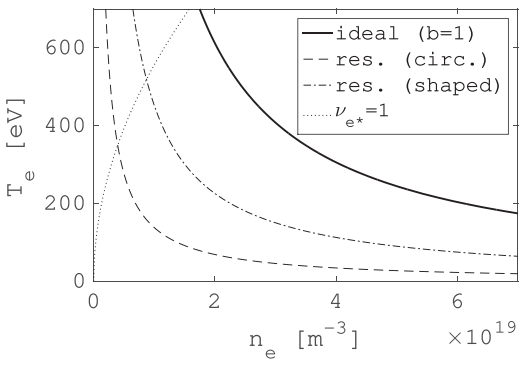

Figure 2. Boundaries for $n = \infty$ ideal ballooning (with $\nu = 0$ where only the first stability boundary is shown) and for a $n = 10$ resistive mode with $s = 1.5$, $R = 3$ m, $B = 4$ T, $\varepsilon = 0.1$, $q = 3$ and $S = 10^7$ for a circular and shaped ($\kappa = 1.5$ and $\delta = 0.3$) tokamak with $T_{\rm i} = T_{\rm e}$. The stability regions lie below each respective curve. The $\nu_{e*} = 1$ level (ν_{e*} is the electron collisionality whose definition follows reference [63] having used $Z_{\rm eff} = 1$) below which (26) is expected to hold is also shown.

ν, we obtain the critical pressure ($q \gg 1$)

$$q\sqrt{\beta}/C = \frac{71}{64}\sqrt{s} + \frac{1}{s}(\varepsilon + \frac{3}{2}e\delta) - \mathscr{U}, \qquad (27)$$

where from (18)

$$\mathscr{U} = -\frac{q|m\omega_{\rm i}|}{\sqrt{s}\pi\omega_{\rm A}}\left(1 - \frac{e}{2} - \frac{10s^2\omega_{\rm A}^3(mS)^{-1}}{\omega_{\rm i}^2|\omega_{\rm e} + \omega_{\rm i}/2|}\right),$$

while from (22) the quantity $\mathscr{U}$ can be written in a form similar to τ defined below equation (26) apart from some slightly different numerical coefficients. In the latter, (27) closely resembles equation (26) expanded to first order in τ in which the ν contribution to b has been neglected. We may drop the second term on the right-hand side of (27) if the magnetic shear is sufficiently large, indicating that for the case with strong diamagnetic effects identified by equation (18) plasma shaping effects are of higher order.

6. Conclusions

In this work the impact of magnetic well contributions, primarily through plasma shaping, also including FLR effects, on the stability properties of RBMs has been analysed. The analysis focussed on a particular choice of the perturbed displacement for which neighbouring Fourier harmonics are translationally invariant (cf (7)). By performing a two scale analysis, with a careful ordering of magnetic shear and shaping contributions, it has been possible to derive an averaged ballooning equation in the ideal and inertial-resistive regions. By matching the two solutions we obtained a dispersion relation which has been analysed for various limiting cases.

When FLR corrections are negligible, stability is generally improved for a vertically elongated cross section with positive triangularity, whereas close to the ideal marginal boundary the growth rate tends to be increased. Diamagnetic effects have a strong stabilising influence altering significantly the growth scaling with the Lundquist number. Various roots and their corresponding stability boundaries, have been identified.

Finally, in the limit of negligible diamagnetic effects, which appears to be appropriate for plasmas near the L $\rightarrow$ H transition, we derived by means of the EPED model an expression of the RBM critical pressure value at the pedestal top. This seems to compare favourably with the type-III ELM dynamics, and thus could provide a sensible physical interpretation for such phenomena.

We point out that our study is limited to the $n \gg 1$ case, for which (7) holds. Therefore, different results might be expected if slightly different forms of the fluid perturbation are considered [64]. Note also that in our calculations we assumed that n is not too large in order for the two scale analysis to hold. Consequently, several effects, which may become important for finite n perturbations, have been neglected. Apart from the obvious modification of the mode structure which requires a global approach as in [65], additional effects would also include variations of temperature and density across the pedestal, neglected in the present work that considers very high-n perturbations. These variations may alter resistivity and diamagnetic flow values around different rational surfaces, yielding a richer dynamics as discussed in [66, 67] As a result, we envisage that for n finite a variational approach, which might be more easily tackled via numerical methods possibly with extended-MHD models, would be more appropriate.

Acknowledgments

This work has been carried out within the framework of the EUROfusion Consortium and has received funding from Enabling Research grant on Reactor Relevant Pedestals (ENR-MFE19.CCFE-04-T002-D001), the Euratom research and training programme 2014–2018 and 2019–2020 under Grant Agreement No. 633053 and from the RCUK (Grant No. EP/T012250/1). To obtain further information on the data and models underlying this paper please contact PublicationsManager@ukaea.uk. The views and opinions expressed herein do not necessarily reflect those of the European Commission. This work was supported in part by the Swiss National Science Foundation.

ORCID iDs

D. Brunetti https://orcid.org/0000-0001-8650-3271
C.J. Ham https://orcid.org/0000-0001-9190-8310
J.P. Graves https://orcid.org/0000-0002-7959-7959
A. Kleiner https://orcid.org/0000-0002-5800-8027

References

[1] Wagner F. *et al* 1984 *Phys. Rev. Lett.* **53** 1453
[2] Keilhacker M. 1987 *Plasma Phys. Control. Fusion* **29** 1401
[3] Leonard A.W. 2014 *Phys. Plasmas* **21** 090501
[4] Viezzer E. 2018 *Nucl. Fusion* **58** 115002
[5] Rapp J. *et al* 2005 *J. Nucl. Mater.* **337–339** 826
[6] Rapp J. *et al* 2009 *Nucl. Fusion* **49** 095012
[7] Rapp J., Kallenbach A., Neu R., Eich T., Fischer R., Herrmann A., Potzel S., van Rooij G.J. and Zielinski J.J. 2012 *Nucl. Fusion* **52** 122002
[8] Sartori R. *et al* 2004 *Plasma Phys. Control. Fusion* **46** 723
[9] ITER Physics Expert Group on Confin Transport ITER Physics Expert Group on Confin Database ITER Physics Basis Editors 1999 *Nucl. Fusion* **39** 2175
[10] Doyle E.J. *et al* 1991 *Phys. Fluids* B **3** 2300
[11] Oyama N. *et al* 2006 *Plasma Phys. Control. Fusion* **48** A171
[12] Connor J.W. 1998 *Plasma Phys. Control. Fusion* **40** 531
[13] Zohm H. 1996 *Plasma Phys. Control. Fusion* **38** 105
[14] Kass T., Günter S., Maraschek M., Suttrop W., Zohm H. and Team A.U. 1998 *Nucl. Fusion* **38** 111
[15] Poli F.M., Sharapov S.E. and Chapman S.C. 2008 *Plasma Phys. Control. Fusion* **50** 095009
[16] Xu X.Q., Dudson B.D., Snyder P.B., Umansky M.V., Wilson H.R. and Casper T. 2011 *Nucl. Fusion* **51** 103040
[17] Orain F. *et al* 2015 *Phys. Rev. Lett.* **114** 035001
[18] Kleiner A., Ferraro N.M., Diallo A. and Canal G.P. 2021 *Nucl. Fusion* **61** 064002
[19] Pogutse O.P. *et al* 1999 *26th EPS Conf. on Plasma Physics* (European Physical Society, Maastricht, Netherlands 14–18 June 1999) vol 23J p 249 (http://ocs.ciemat.es/EPS1999/web/pdf/p1036.pdf)
[20] Chankin A.V. and Saibene G. 1999 *Plasma Phys. Control. Fusion* **41** 913
[21] Strauss H.R. 1981 *Phys. Fluids* **24** 2004

[22] Connor J.W., Hastie R.J., Wilson H.R. and Miller R.L. 1998 *Phys. Plasmas* **5** 2687
[23] Sykes A., Bishop C.M. and Hastie R.J. 1987 *Plasma Phys. Control. Fusion* **29** 719
[24] Bishop C.M., Hastie R.J., Sykes A. and Wilson H.R. 1990 *Phys. Fluids* B **2** 3052
[25] Correa-Restrepo D. 1982 *Z. Naturforsch.* A **37** 848
[26] Correa-Restrepo D. 1985 *Plasma Phys. Control. Fusion* **27** 565
[27] Drake J.F. and Antonsen T.M. 1985 *Phys. Fluids* **28** 544
[28] Glasser A.H., Greene J.M. and Johnson J.L. 1975 *Phys. Fluids* **18** 875
[29] Krymskii A.M. 1981 *Sov. J. Plasma Phys.* **7** 371
[30] Lütjens H., Bondeson A. and Vlad G. 1992 *Nucl. Fusion* **32** 1625
[31] Saibene G. *et al* 2002 *Plasma Phys. Control. Fusion* **44** 1769
[32] Snyder P.B., Groebner R.J., Leonard A.W., Osborne T.H. and Wilson H.R. 2009 *Phys. Plasmas* **16** 056118
[33] Snyder P.B., Groebner R.J., Hughes J.W., Osborne T.H., Beurskens M., Leonard A.W., Wilson H.R. and Xu X.Q. 2011 *Nucl. Fusion* **51** 103016
[34] Brunetti D., Ham C.J., Graves J.P., Wahlberg C. and Cooper W.A. 2020 *Plasma Phys. Control. Fusion* **62** 115005
[35] Migliuolo S. 1993 *Nucl. Fusion* **33** 1721
[36] Migliuolo S., Pegoraro F. and Porcelli F. 1991 *Phys. Fluids* B **3** 1338
[37] Hazeltine R.D. and Meiss J.D. 1992 *Plasma Confinement* (Reading, MA: Addison-Wesley)
[38] Ara G., Basu B., Coppi B., Laval G., Rosenbluth M.N. and Waddell B.V. 1978 *Ann. Phys.* **112** 443
[39] Miller R.L., Chu M.S., Greene J.M., Lin-Liu Y.R. and Waltz R.E. 1998 *Phys. Plasmas* **5** 973
[40] Shafranov V.D. and Yurchenko E.I. 1968 *Nucl. Fusion* **8** 329
[41] Mikhailovskii A.B. 1998 *Instabilities in a Confined Plasma* (Bristol: Institute of Physics Publishing)
[42] Tsang K.T. 1981 *Phys. Fluids* **24** 2017
[43] Coppi B., Greene J.M. and Johnson J.L. 1966 *Nucl. Fusion* **6** 101
[44] Connor J.W., Hastie R.J. and Taylor J.B. 1978 *Phys. Rev. Lett.* **40** 396
[45] Mikhailovskii A.B. and Yurchenko E.I. 1982 *Plasma Phys.* **24** 977
[46] Snyder P.B. *et al* 2002 *Phys. Plasmas* **9** 2037
[47] Fu G.Y., Van Dam J.W., Holland D.L., Fried B.D. and Baños A. 1990 *Phys. Fluids* B **2** 2623
[48] Newcomb W.A. 1960 *Ann. Phys.* **10** 232
[49] Connor J.W. *et al* 1991 *Phys. Fluids* B **3** 1539
[50] Lortz D. and Nührenberg J. 1979 *Nucl. Fusion* **19** 1207
[51] Pogutse O.P. *et al* 1980 *Sov. J. Plasma Phys.* **6** 341
[52] Coppi B., Ferreira A. and Ramos J.J. 1980 *Phys. Rev. Lett.* **44** 990
[53] Antonsen T.M. Jr, Ferreira A. and Ramos J.J. 1982 *Plasma Phys.* **24** 197
[54] Connor J.W., Ham C.J. and Hastie R.J. 2016 *Plasma Phys. Control. Fusion* **58** 085002
[55] Wolfram Research Inc. 2010 *Mathematica Version 6.0* (Champaign, IL: Wolfram Research Inc.)
[56] Hazeltine R.D. and Ross D.W. 1978 *Phys. Fluids* **21** 1140
[57] Hastie R.J., Ramos J.J. and Porcelli F. 2003 *Phys. Plasmas* **10** 4405
[58] Abramowitz M. and Stegun I.A. 1964 *Handbook of Mathematical Functions* (New York: Dover)
[59] Porcelli F. 1987 *Phys. Fluids* **30** 1734
[60] Snyder P.B. *et al* 2004 *Nucl. Fusion* **44** 320
[61] Riva F., Lanti E., Jolliet S. and Ricci P. 2017 *Plasma Phys. Control. Fusion* **59** 035001
[62] Seto H., Yagi M., Aiba N., Matsuyama A., Dudson B.D. and Xu X. 2018 *Plasma Fusion Res.* **13** 3403086
[63] Sauter O., Angioni C. and Lin-Liu Y.R. 1999 *Phys. Plasmas* **6** 2834
[64] Tsang K.T. and Catto P.J. 1977 *Phys. Rev. Lett.* **39** 1664
[65] Brunetti D., Graves J.P., Lazzaro E., Mariani A., Nowak S., Cooper W.A. and Wahlberg C. 2018 *Nucl. Fusion* **58** 014002
[66] Hatch D.R. *et al* 2021 *Nucl. Fusion* **61** 036015
[67] Larakers J.L., Curie M., Hatch D.R., Hazeltine R.D. and Mahajan S.M. 2021 *Phys. Rev. Lett.* **126** 225001